Industrial TCOs for SHJ solar cells: Approaches for optimizing performance and cost

Alexandros Cruz[1], Darja Erfurt[1], René Köhler[2], Martin Dimer[2], Eric Schneiderlöchner[2] & Bernd Stannowski[1]

[1]Helmholtz-Zentrum Berlin, PVcomB, Berlin, Germany; [2]VON ARDENNE GmbH, Dresden, Germany

Abstract

Silicon heterojunction (SHJ) solar cell technology is an attractive technology for large-scale production of solar cells with a high conversion efficiency beyond 24%. One key element of SHJ solar cells, contrasting with today's widespread passivated emitter and rear contact (PERC) cell technology, is the use of transparent conductive oxide (TCO), which poses challenges in performance and costs but also presents opportunities. This paper discusses these aspects and shows the potential for improving cell efficiency at reduced cost by using new TCOs deposited by direct current (DC) sputtering. In the case of rear-junction SHJ cells, it is possible to reduce, or even avoid, indium usage in such TCOs, with aluminium-doped zinc oxide (AZO) being one possible substitute for indium-oxide-based TCOs. The availability of high-performance TCOs for large-scale mass production, which will encourage the market penetration of SHJ cells, is summarized.

Introduction

Silicon solar cells based on passivated emitter and rear contact (PERC) technology have reached multi-gigawatt levels in mass production, with conversion efficiencies (CEs) of 22% and now approaching 23%. For even higher CEs, passivated contacts are considered to be the next generation of cell technology. Here, silicon heterojunction (SHJ) technology is a promising candidate and is racing out of the starting gate, with a CE of 23–24% having already been demonstrated on full-size wafers, not only in pilot lines but also in large-scale production [1]. While it was Panasonic (formerly Sanyo) who pioneered this technology, various players worldwide have in the meantime been building up their own production lines, such as ENEL Green Energy and Hevel Solar in Europe, and REC, Jinergy, GS-Solar and various others in Asia.

The major benefits of SHJ technology were discussed in a recent article by Ballif et al. [2]. Besides the high CE, a key advantage of SHJ is the lean production sequence, with only four main steps required for processing both sides symmetrically:

1. Wet-cleaning and texturing of wafers.
2. a-Si:H deposition by plasma-enhanced chemical vapour deposition (PECVD).
3. Deposition of transparent conductive oxide (TCO) layers by physical vapour deposition (PVD, usually sputtering).
4. Screen printing of silver grids.

Because of the low-temperature (<200°C) processes and the symmetrical device stack, stress-induced wafer bending and cracking can be avoided, which means *thin* wafers can be utilized, thus saving material costs and energy. The SHJ stack occurs naturally in a bifacial cell design; moreover, SHJ cells have the lowest temperature coefficient in the field, typically –0.28%/°C. The combination of bifaciality and low temperature coefficient increases the energy yield of a PV system.

On the other hand, some of the factors limiting a rapid increase in the uptake of SHJ technology are the relatively high equipment costs, mostly for PECVD (but also for PVD), and the adapted cell contacting for module manufacturing (no standard high-temperature soldering). More Ag paste is needed than for standard Si cells, because of the low-temperature curing, yielding lower-conductivity fingers; this, however, depends on the interconnection approach, specifically whether or not busbars are used. Finally, and discussed in more detail in this paper, targets for sputtering the TCO layers on both sides are required, which are costly for the materials that are usually employed.

Indium oxide (In_2O_3) doped with tin (Sn), referred to as *ITO*, is currently the most commonly used TCO [3–5]. This transparent conductive oxide is well known from the mass production of flat-panel displays (FPD) and exhibits suitable opto-electronic properties, such as low resistivity of thin layers and sufficient transparency in the visible range. An important consideration for FPD production, *ITO* can be processed by photolithography, as it is etchable (in the as-deposited state) and is long-term stable after solid-phase crystallization upon thermal annealing at 150–200°C. Generally, ITO is deposited by direct current (DC) magnetron sputtering on large areas. Even though DC sputtering initially causes some damage of the silicon surface passivation, this is fully annealed at temperatures of around 200°C, which is reached either during sputtering or later during curing of the Ag paste after screen printing.

In contrast to FPDs, TCO has to fulfil additional

requirements when applied to the front side of SHJ cells, namely an excellent transparency in the wider wavelength range 300–1,100nm. Fig. 1 shows the absorption spectra of various TCO layers, demonstrating the differences in parasitic absorption in the short- and long-wavelength regimes. Besides this low absorption, low contact resistances with both the n- and p-doped silicon layers, as well as with the metal grid, are mandatory for the TCO layers on both sides.

Last, but not least, the cost constraints of solar cells are extremely stringent, and, to envision PV on a terawatt scale, it is essential to reduce (or better still, avoid) the use of critical or scarce materials, such as indium (In). The latter aspect, however, is still difficult to address, as most device-quality TCOs contain indium. One option is to decrease the thickness of such TCOs, which then requires a second layer to be deposited in order to maintain ideal optical (anti-reflective) performance. This, in turn, increases the number of process steps and, hence, the process complexity and costs.

For the replacement of indium in TCOs, on the other hand, aluminium-doped zinc oxide (AZO) is one of the very few alternative candidates which is considered. As will be discussed in this paper, although this option is an attractive, low-cost and abundant alternative, one has to cope with lower conductivity and poor long-term stability.

This paper addresses the optimization of TCO for incorporation in SHJ solar cells. A metric is presented for evaluating and benchmarking different TCOs with regard to their suitability for application in SHJ cells. To reduce the optical loss in the front TCO, the use of materials with a high transparency is mandatory. A high charge-carrier mobility, typically >100cm^2/Vs, allows a reduction in carrier density (at constant resistivity), thereby reducing the optical loss due to free-carrier absorption (FCA).

Various 'high-mobility' TCO materials based on indium oxide with different dopings have been investigated in the past [6–13]. All of these exhibit excellent properties as TCO layers on glass and most of them a high CE as well. Target manufacturing, however, is difficult and the costs are high for many of these materials.

New TCOs that can be processed in large-scale production from rotatable targets are now available, yielding high mobility and producing SHJ cells with high CE. The circumstances under which AZO as an indium-free and low-cost alternative can be implemented in high-efficiency SHJ cells will be discussed later. A cost comparison of In-based and ZnO-based targets will also be presented.

TCO for SHJ solar cells

In the past, several TCO materials have been investigated for use in SHJ solar cells. Important requirements for this implementation are high conductivity and high transparency, with processing temperatures below 200°C (because of the sensitivity of thin-film silicon passivation layers), as well as good contact formation with the neighbouring layers [14].

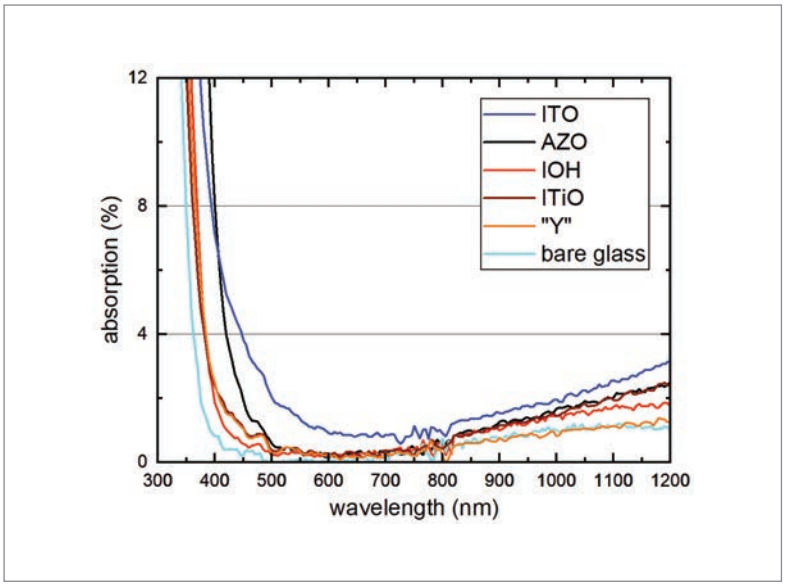

Figure 1. Optical absorption spectra for various types of TCO layer of thickness 100±10nm on glass substrate for implementation in SHJ cells.

Among some of the relevant TCOs, polycrystalline Sn-doped In_2O_3 (ITO) grown at temperatures below 200°C, which reaches electron mobility (μ_e) around 40cm^2/Vs [3–5], has found wide application in SHJ solar cells. In-based TCOs doped with other metals, such as titanium (Ti) [15,16], zirconium (Zr) [6,12,13], molybdenum (Mo) [15,17–19] and tungsten (W) [10,11], yield μ_e values greater than 80cm^2/Vs at a charge-carrier density (n_e) ranging from 1×10^{20} to 3×10^{20}cm^{-3}. These layers can be deposited via magnetron sputtering, pulsed laser deposition (PLD), and ion plating with DC arc discharge or reactive plasma deposition (RPD). Out of these, sputtering is the most established method for mass production. An even higher mobility of μ_e >100cm^2/Vs can be achieved for solid-phase crystallized (SPC) hydrogen (H)-doped In_2O_3 (IOH) [6–9] and cerium (Ce) ICeO:H [7] films with $1\times10^{20} < n_e < 3\times10^{20}$cm^{-3}. These films are deposited at low temperatures in an amorphous matrix and subsequently annealed at temperatures above 150°C, which results in high μ_e values because of the formation of large grains.

The TCOs introduced above are attractive because of their outstanding opto-electrical performance, but to date mainly ITO and IWO:H have found their way into industrial production. The scarcity of indium, however, is a motivation for the implementation of alternative TCOs. AZO offers the advantage of having more abundant composite materials. AZO layers with a thickness of several hundred nanometres,

"To envision PV on a terawatt scale, it is essential to reduce the use of critical or scarce materials, such as indium."

TCO	Sheet resistance range	Sheet resistance $R_{\square}$ @ t=75nm [Ω]	Electron mobility μ_e [cm²/Vs]	Carrier concentration n_e [10^{20}cm^{-3}]
ITiO, IOH, ICeO:H, IWO:H	Low-$R_{\square}$	40–70	80–120	1.5–2.0
ITO, IZO	Mid-$R_{\square}$	70–190	30–60	1.5–2.0
AZO	High-$R_{\square}$	170–370	15–25	1.5–2.0

Table 1. Comparison of the electrical properties of different TCOs.

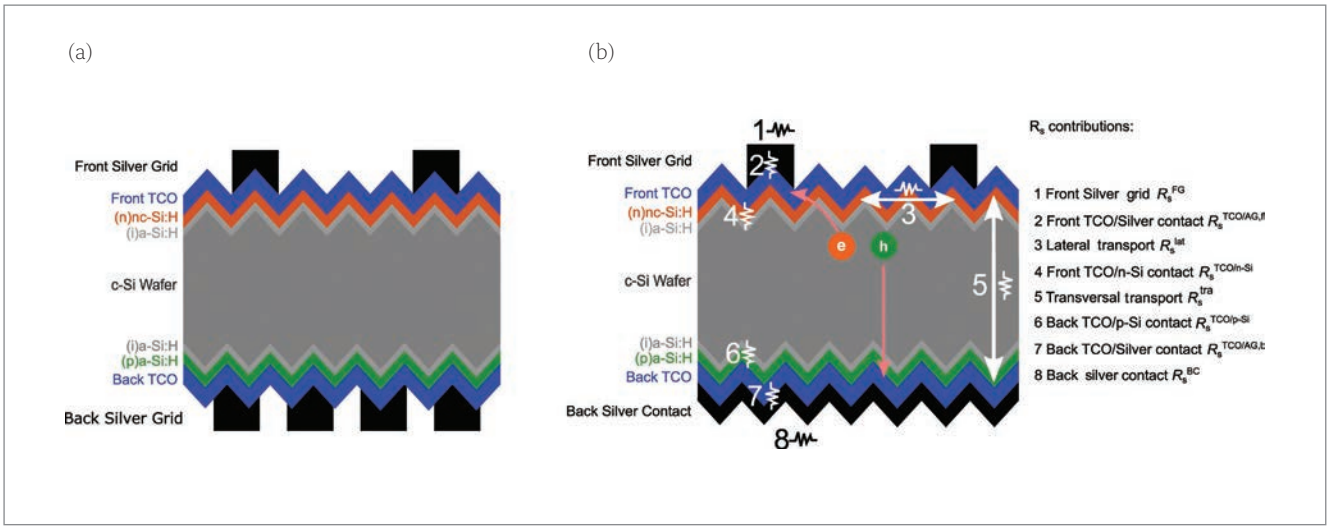

Figure 2. Schematic cross-sectional views of rear-junction silicon heterojunction (SHJ) solar cells: (a) bifacial cell design; (b) monofacial cell design, with the series resistance (R_s) components shown.

sputtered at elevated temperatures >250°C, yield good opto-electronic properties [20] and also stability [21]. Thin layers of thickness less than 100nm deposited at temperatures below 200°C, as required for SHJ cells, in contrast exhibit a poor crystal structure, consequently resulting in low mobility values around 20cm²/Vs and poor long-term stability [22]. Improved stability for SHJ solar cells, however, has been shown by applying an amorphous silicon oxide (a-SiO_2) capping [23].

As indicated by the μ_e values obtained, and depending on processing conditions, the different TCOs demonstrate a wide range of electron mobilities. The TCO sheet resistance ($R_{\square}$) ranges can be classified as shown in Table 1. Here, a carrier concentration range $1.5\times10_{20} < n_e < 2.0\times10^{20}$cm^{-3} is considered: this represents a good compromise for achieving low FCA, good electrical conductivity and good contact formation with neighbouring layers, and a 75nm TCO thickness for anti-reflective properties.

The symmetry in SHJ cell processing and the usage of (n-type) wafers with very high carrier lifetimes allows one to freely choose which contact (n or p) faces the front. The position of the p contact (junction) has an impact on the optimization of the front TCO for obtaining both high transparency and low series resistance R_s of the cell [24–27]. To demonstrate this, Fig. 2 shows schematic cross sections of bifacial and monofacial SHJ solar cells in a rear-junction configuration with all R_s contributions indicated. A detailed analysis of R_s components and of their contributions in SHJ solar cells can be found in Basset et al. [25] and Wang et al. [28]. The high conductivity, i.e. density and mobility, of electrons in the c-Si wafer, along with the very low contact resistance of the n/TCO contact, favours the choice of the n contact being on the front ('rear junction'), as the lateral current transport is significantly supported by the wafer. This relaxes the conductivity requirement of the TCO (sheet resistance), thus allowing an optimization towards highest transparency.

To illustrate the effect of the above-mentioned freedom in cell design, Fig. 3 presents simulated R_s curves together with experimental values extracted from solar cells, with an ITO process variation as a function of the front-TCO sheet resistance. The experimental values validate the trends of the model [27]. As can clearly be seen, the rear-junction design offers an advantage for high-resistive TCOs by benefiting from the lateral support in electron conduction in the Si wafer. The front-junction design, on the other hand, is more favourable for low-resistivity TCO layers; this design takes advantage of the lower *transversal* R_s contribution, since electrons, having higher mobility than holes, travel to the rear of the wafer (with photogeneration mainly occurring close to the front side). The trade-off between the lateral and transversal R_s contributions will determine which solar cell design is most suitable, depending on the available TCO sheet resistance.

The $R_{\square}$ ranges for different TCOs reported in the

literature and as defined in Table 1 are shown in Fig. 3 with the corresponding colour shading. TCOs with low $R_{\square}$ (red) are more beneficial when implemented in a front-junction device, while TCOs with mid-range $R_{\square}$ (blue) are in a transitional region where the R_s difference between front-junction and rear-junction devices is fairly small. In contrast, TCOs with high $R_{\square}$ (grey) are clearly advantageous when implemented in a rear-junction design; this is favourable for AZO, for example, with it being highly transparent but not very conductive, yet still producing the same SHJ cell efficiency >23% as the ITO reference cell [23]. At the Helmholtz-Zentrum Berlin, SHJ solar cells with both ITO- and AZO-based front TCO have achieved a certified CE above 23.5% [29].

Another approach that takes advantage of the wafer lateral transport support, demonstrated by some research groups [27,30] and in pilot production [31], is to implement *thinner* TCOs, which reduces parasitic absorption, thus maintaining or improving solar cell CE. The implementation of a thinner TCO layer, however, requires a second layer on top – for example, SiO_2 or Si_3N_4 – to maintain the anti-reflection (AR) optimum [32–34].

To accurately quantify the optical performance of different TCOs when implemented in the cell stack, i.e. determine the specific loss in short-circuit current density (J_{sc}), simulations with a ray-tracing software tool (GenPro4 [35]) were carried out. Taking into account the TCO-related power loss in the cell due to both an increase in R_s and a decrease in J_{sc}, different TCO materials were benchmarked, as shown in Fig. 4. For this purpose, a reference solar cell with CE = 23.3% was considered, without TCO-related losses in J_{sc} and R_s (*FF*). IOH, ITO and AZO were studied as examples of the low-$R_{\square}$, mid-$R_{\square}$ and high-$R_{\square}$ regimes respectively.

Implementations of both standard 75nm-thick ('thick') and optically optimized thinner ('thin') TCOs were studied. For a fair comparison (i.e. to stay in the AR optimum in every case), *all* cells (with 'thick' and 'thin' TCOs) were finished with an a-SiO_2 capping layer. The contact resistivities at the TCO/Ag and TCO/Si interfaces were assumed to be (low and) equal for all three TCOs, which, of course, is a simplification. This will be discussed later and is presented in Haschke et al. [36]. Further details of the optimized layer thicknesses and simulation results can be found in Cruz et al. [27].

The graphs in Fig. 4 show the TCO-related power loss due to a decrease in J_{sc} and to an increase in R_s, for rear-junction (Fig. 4(a)) and front-junction (Fig. 4(b)) devices. Clearly, the IOH outperforms the other two TCOs because of its outstanding opto-electronic properties in both cases. In Fig. 4(a), showing the thick ITO and AZO, the materials compensate their CE losses, since the lower-conductivity AZO shows lower parasitic absorption than the ITO. When this is compared with the thinner versions of TCOs, it can be observed that the CE loss slightly decreases as a result of reduced TCO parasitic absorption. The ITO clearly benefits more from this thinning, because of its comparably higher parasitic absorption, ultimately leading to a slightly better CE than with AZO. This shows that thinner TCOs with improved optics can be implemented in a rear-junction configuration and will be beneficial in terms of CE.

In contrast, looking at the front-junction design in Fig 4(b), it can be seen that the high-conductivity IOH will not suffer from the lower lateral transport contribution by the wafer. The lower-conductivity ITO and AZO, however, increase the resistive losses. Decreasing the thickness of the ITO does not lead to a CE advantage, whereas in the case of the AZO it is clearly disadvantageous. It can be concluded that a high-conductivity TCO, here IOH in the example, can be implemented on both rear- and front-junction solar cell configurations without major differences in CE losses. Lower-conductivity TCOs – such as ITO and AZO – will suffer from the higher lateral R_s present in the front-junction configuration. Thinning the TCO on rear-junction solar cells is advantageous if the TCO exceeds a certain absorption threshold, even for a TCO with low conductivity, here AZO in the example. In a front-junction design, the thinning will only bring small benefits, or may even be disadvantageous for lower-conductivity TCOs such as AZO.

Performance of industrial high-mobility TCOs

In order to test high-mobility TCOs sputtered at a high rate by DC sputtering from tube targets, as

"SHJ solar cells with both ITO- and AZO-based front TCO have achieved a certified CE above 23.5%."

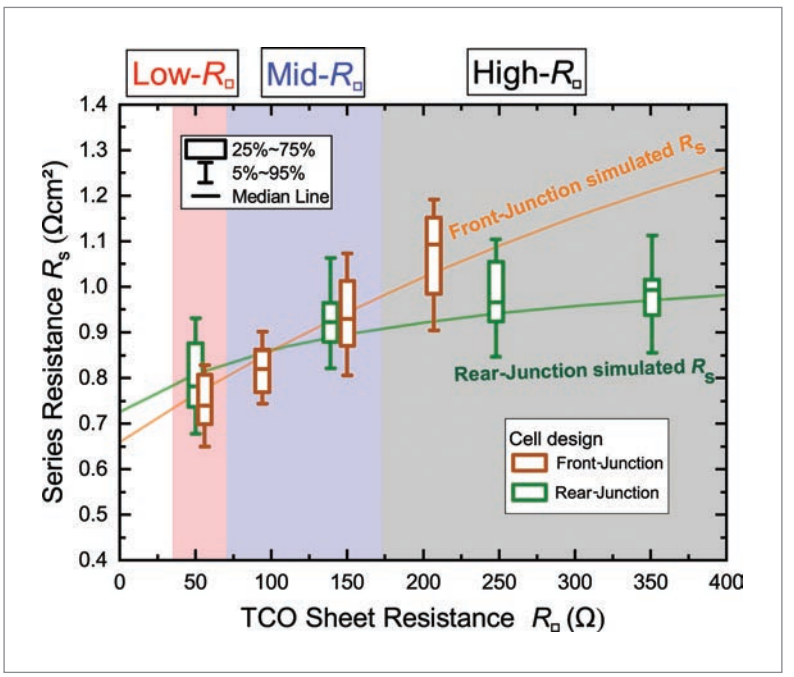

Figure 3. Series resistance versus front-TCO sheet resistance for front- and rear-junction SHJ solar cells. The curves represent simulated results, while the boxes indicate results for measured cells with an ITO variation.

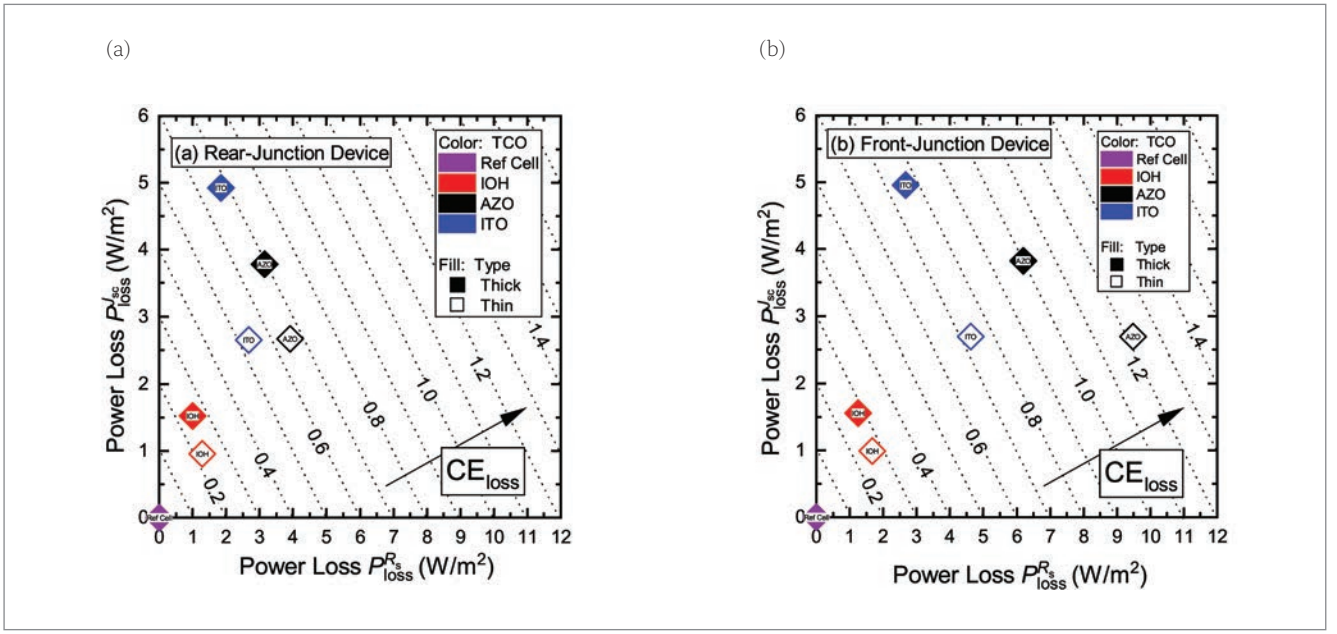

Figure 4. Current-density-related power loss (P_{loss}^{J}) and series-resistance-related power loss (P_{loss}^{R}) for (a) rear-junction and (b) front-junction SHJ cells. Conversion efficiency (CE) loss values are indicated by the dashed lines; these losses are relative to a reference solar cell with 23.3% CE, represented by the purple diamond at (0,0). The filled symbols represent 75nm-thick TCOs (standard) but with an anti-reflection coating (ARC) on top, while the open symbols represent thinner (optimized) TCO layers, also with an ARC.

performed in large-scale mass production, different materials were used for the front TCO in bifacial rear-junction SHJ solar cells. Two types of high-mobility TCO were tested, namely titanium-doped indium oxide (ITiO) and indium oxide with an undisclosed doping type ('Y'). Additionally, ITO with various doping concentrations was tested, namely containing 97% indium oxide and 3% tin oxide in the target ('97/3') and ITO 99/1. As the reference material, ITO 97/3 was implemented on the rear side of all cells. A group of cells with ITO 95/5 on both front and rear sides was also included.

Corresponding test layers on glass revealed TCO sheet resistances in the range 36–136Ω after deposition and annealing for 30 min at 200°C under ambient conditions, which is comparable to the curing carried out after screen printing. This is a suitable range for the implementation as the front contact in rear-junction SHJ solar cells, as discussed earlier (see Fig. 3). It must be taken into account, however, that TCO layers deposited on glass might exhibit properties (carrier mobility) different from those when the layers are deposited on silicon, as required for solar cells. This has been attributed to two effects [29]: (1) different crystal nucleation and, hence, grain structure; (2) different hydrogen content which diffuses from the silicon layer into the TCO.

The ITiO and Y layers exhibit high mobilities of up to 90cm²/Vs, but with different charge-carrier densities, namely 2×10^{20}cm^{-3} and ~0.8×10^{20}cm^{-3} respectively. For ITO97/3 and ITO99/1 films, lower mobility values, of around 60 and 70cm²/Vs at charge-carrier densities of 2.7×10^{20}cm^{-3} and 1.8×10^{20}cm^{-3} respectively, were measured. As a result of the very low charge-carrier density, the Y films showed the lowest parasitic absorption in the near-infrared region (see Fig. 1), which makes this material the most promising for achieving the highest J_{sc} and, possibly, the highest CE in solar cells.

The *I–V* parameters of each of the test groups are shown in Fig. 5. All cells exhibit comparable open-circuit voltages (V_{oc}), with medians in the narrow range of 737–738mV. This confirms that the passivation did not degrade because of different sputter damage. As expected, the solar cells with high-mobility TCOs yielded the highest J_{sc} values, with medians of 39.0mA/cm² and 39.2mA/cm² for ITiO and Y respectively. This is up to 0.5mA/cm² higher than that achieved with the reference ITO97/3.

Despite the high J_{sc} and good V_{oc} values, however, the cells with a Y-front contact did not produce the highest efficiencies. The highest median CE of 22.9% was actually obtained for ITO99/1, while the highest value of CE of 23.3% was measured for a cell with ITiO. The lower CE in the case of the Y samples results from the lower median *FF* of only around 77%, which is due to a value of R_s that is considerably higher; in fact, the cells with a Y-front contact yield the highest median R_s values of 1.3–1.6Ωcm². In contrast, the median R_s value is 0.9Ωcm² for the ITO99/1 cells, resulting in a significantly higher median *FF* of 79.5%.

Importance of low contact resistance

The high series resistance of the cells with (low carrier density and) high-mobility TCO is in fact an aspect which needs to be tackled. More precisely, the two main components of R_s here are the contact resistance of the TCOs with the n- and p-doped silicon contact layers, which have been investigated in detail in the literature

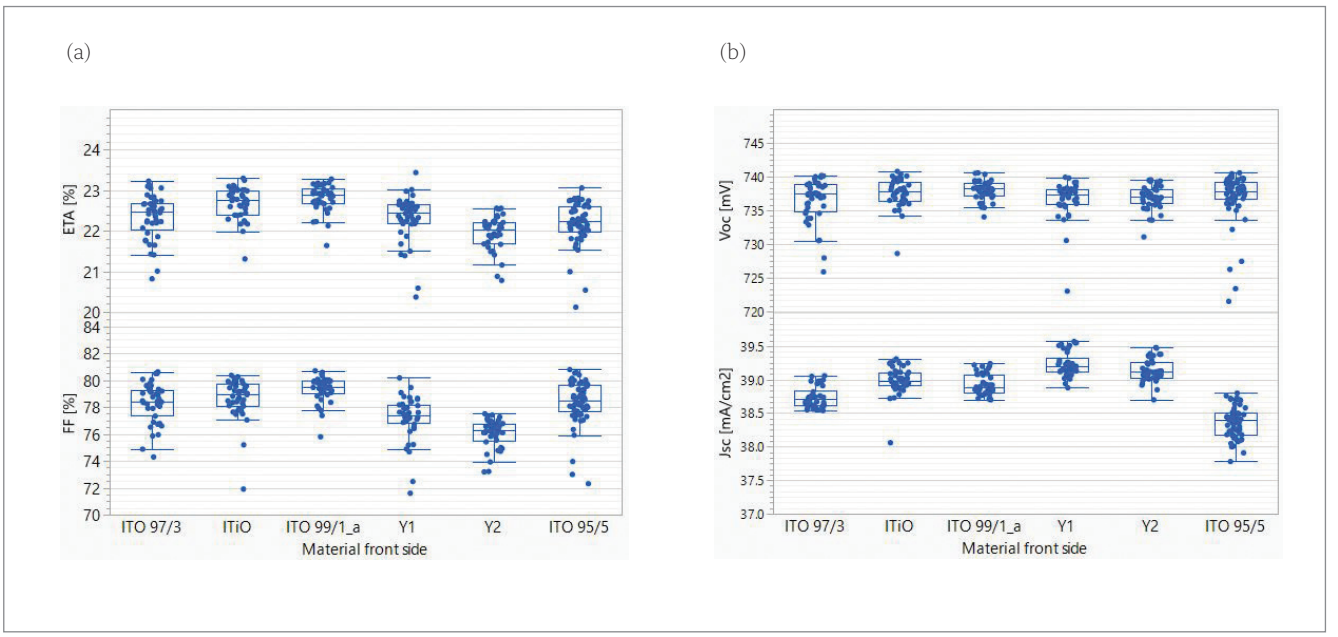

Figure 5. *I–V* parameters of 4cm²-sized bifacial SHJ solar cells with various front TCOs and ITO 97/3 on the rear side. ITO 95/5, DC sputtered from a tube target at HZB, was included as a reference.

[37–40]. In the case of n-doped c-Si-based solar cells, the contact resistance of the TCO with the n-doped Si layers can be characterized by various, relatively simple, techniques, such as the Cox and Strack [41] or transmission-line [42] methods. The contact resistance of the TCO with the p-doped Si layer (TCO/p), in contrast, is more difficult to access, because a junction is formed. As shown by Basset et al. [21] and Wang et al. [24], for example, a simple method for extracting the value of the R_s component is to derive all the accessible components of R_s, and the remaining value is then concluded to be the TCO/p contact resistance.

The contact resistivity ρ_c depends on the detailed band alignment and band bending, as well as on the interface defect states; hence, several parameters are important, specifically the activation energy of the doped Si layer and the charge-carrier density, but also the work function difference between both materials. Procel et al. [38] showed that ρ_c is minimal when the doped layers exhibit low activation energy values, such as those obtained with nanocrystalline silicon layers instead of amorphous layers. Moreover, the charge-carrier density of the TCO should be well above 1×10^{20}cm^{-3}; this is particularly important for the TCO/p contact, for which efficient recombination of hole and electrons at the contact is essential. With regard to the selection and optimization of TCO layers, this entails finding an optimum for n_e, which must be high enough to achieve sufficiently low ρ_c values, but, at the same time, must be as low as possible in order to limit parasitic absorption (FCA).

In a more recent experiment, a Y layer with a higher carrier density was selected; Fig. 8 shows the properties available by tuning the process. Indeed, for the adapted TCO, the cell *FF* recovered, but at the cost of a small decrease in J_{sc} because of the additional FCA. Overall, CE still increased up to a similar level to that found for the best groups in Fig. 5, which demonstrates the importance of careful tuning of the layer and interface properties.

Industrial aspects: target costs

The common types of TCO target used in the crystalline silicon PV industry are *rotatable targets*, which are cylindric shells of the TCO material bonded on a backing tube made of metal. The longer the tube, the more shells must be used for the tube target. The reason why the industry prefers this type of target for sputtering of TCOs is the much higher utilization rate of the TCO target material than that for planar types of TCO target. The utilization rate of the target material achievable with a rotatable target is usually ≥80%; this is of particular interest in the case where TCO materials are expensive, such as indium-based TCOs. As regards TCOs in the crystalline silicon PV industry, indium-based TCOs are dominant owing to their excellent layer properties (as was also shown earlier). Nevertheless, some market players are also offering zinc-based TCOs for the same purpose. Indeed, there are advantages and disadvantages for using zinc-based TCOs. One advantage is the lower cost of a zinc-based tube target of dimensions identical to those of an indium-based target, whereas the lower conductivity of zinc presents some constraints in solar cell design, as discussed earlier and visualized in Fig. 3.

Fig. 6 shows the specific target cost per cm³ of tube targets for zinc-based TCOs and indium-based TCOs; note that the cost of the backing tube is

"The high series resistance of the cells with (low carrier density and) high-mobility TCO is an aspect which needs to be tackled."

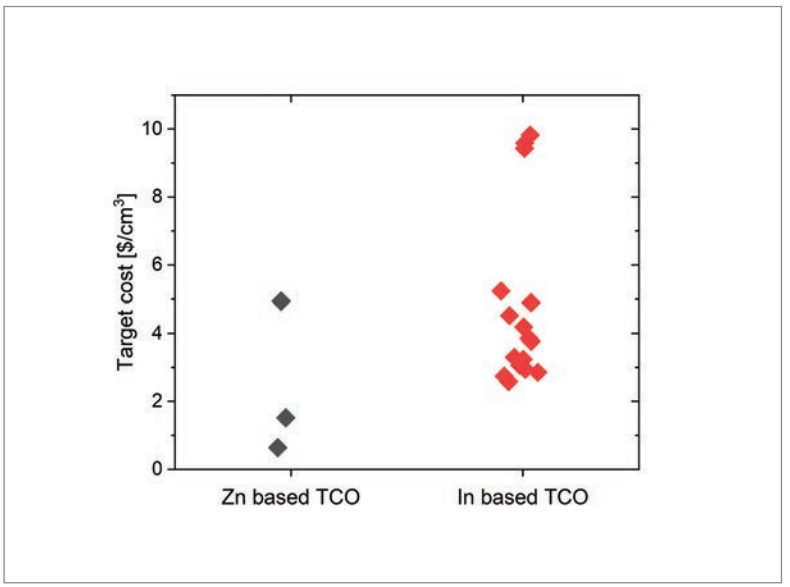

Figure 6. Specific target cost per cm³ of target material for indium-based and zinc-based TCOs.

"Zn-based TCOs can be around a quarter the price of In-based TCOs."

excluded from the target cost. The data points were collected from target suppliers all around the world. The smaller number of data points for zinc-based TCOs can be attributed to the lack of interest for that material shown by the crystalline silicon PV industry so far.

Some scattering in target cost exists because of the different materials within the zinc group and within the indium group, or because of different suppliers. The data points denoting higher target cost in both groups can be explained by less common compositions and/or costly manufacturing processes and/or high margins. The lower-cost data points observed in both groups should be representative cost values for solar cell producers with several hundreds of yearly tube targets demand.

A comparison of the lowest value in both groups reveals that Zn-based TCOs (target cost ~$0.6/cm³) can be around a quarter the price of In-based TCOs (target cost ~$2.6/cm³). It should be pointed out, however, that these data points are a snapshot of the present situation and will soon probably become obsolete, depending on the volatility of the stock market with regard to feedstock material, in particular indium.

Industrial aspects: TCO mass production

Besides the desire to implement indium-free TCOs with the aim of improving operational expenditure (OPEX), it is in the best interest to have a high-volume manufacturing sputtering tool which can produce a high-quality TCO coating at a low cost. Fig. 7 shows the highly productive XEA|nova L sputtering system from VON ARDENNE, which can deposit TCO layers at a throughput of 8,000 M6 wafers per hour in the basic version, and at an even higher throughput by using upgrade packages.

During 2019 the XEA|nova equipment became part of an industrial manufacturing line reaching top cell efficiencies of above 24% using TCO films similar to the ones investigated here.

In order to achieve a high throughput, the deposition rate of the TCO layers must be high, which can be realized by applying a high DC power to the tube target. However, the TCO properties still have to be maintained when TCO is prepared at higher power densities. Fig. 8 shows the electron mobilities and charge-carrier densities of TCO films, sputtered at 4kW and 8kW from ceramic tube targets of TCO type 'Y'. High mobilities of around 80cm²/Vs could be achieved at a power level of 4kW after

Figure 7. Example of TCO mass-production equipment: VON ARDENNE's XEA|nova L.

deposition. An increase of the sputtering power to 8kW reduces the maximum mobility by a maximum of 10%. It is interesting that the mobilities could be further increased, up to 100cm²/Vs, by annealing the films for 30 min at 200°C, as shown in Fig. 8.

Conclusions

SHJ solar cell technology has demonstrated to be an important player on the way to increasing its share in large-scale production. This is because of the very high conversion efficiencies achieved and the lean production process.

Regarding the role of TCOs, three aspects still need to be addressed to boost SHJ technology's prospects of making additional inroads into the solar cell industry:

1. **Further improve cell performance.** This can be achieved by the implementation of high-mobility TCOs which are suitable for mass production. It was shown that high-mobility TCOs can be sputtered at high throughputs, and these TCOs were tested in SHJ solar cells. Although the CE of such SHJ cells is high, it still lags behind that of reference cells with the best ITO front TCO, despite a lower absorption and higher mobility This is attributed to an increased contact resistivity of the TCOs with the n- and/or p-doped silicon contacts. Fine-tuning of the TCO and the implementation of contacting layers and/or interface optimization will need to be addressed in order to further reduce resistive losses at these interfaces and, thereby, reap the full benefits of the superior TCO properties.

2. **Reduce usage of scarce (and expensive) materials, particularly indium.** An attractive option for realizing a saving in material cost is to decrease the TCO thickness; this is even more attractive with costly high-conductivity (high-mobility) TCOs. However, another process step is needed to deposit a second, anti-reflective (capping), layer (ARC) on top of the TCO in order to reduce reflection losses. Alternatively, as shown in this paper, lower-conductivity TCOs (AZO in the example given) can be implemented in rear-junction solar cells without compromising on CE. This gains relevance where cost is concerned: in the analysis presented, ZnO-based targets demonstrate lower cost at $0.6/cm³ for target material, compared with $2.6/cm³ for In-based targets. The limited stability of AZO can be dealt with by, for example, capping it with a dielectric layer (a-SiO_2 or a-SiN_x).

3. **Reduce PVD equipment costs.** Scaling and increasing the throughput of TCO production lines is the way to go, with DC sputtering being ready for high-throughput production of high-performance TCOs.

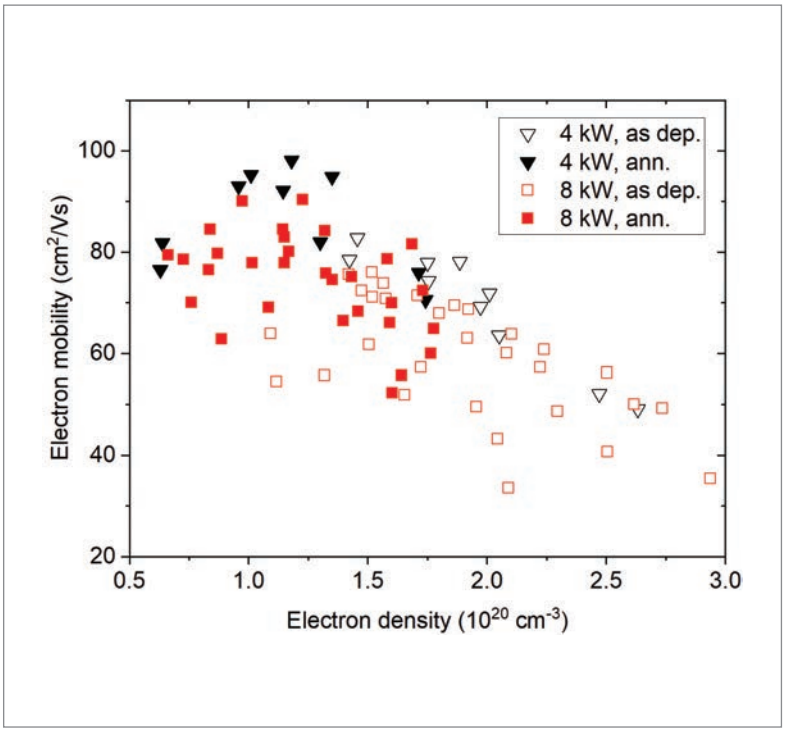

Figure 8. Electrical properties of TCO layers sputtered at 4kW and 8kW from ceramic tube targets of TCO type 'Y', in the as-deposited state and after annealing for 30 min at 200°C in ambient conditions.

Acknowledgements

Funding by the German federal ministry for economic affairs and energy (BMWi) within the framework of the Dynasto project under #0324293 is gratefully acknowledged.

References

[1] Chunduri, S.K. & Schmela, M. 2019, "Heterojunction solar technology", *Taiyang News* [http://taiyangnews.info/TaiyangNews_Report_Heterojunction_Solar_Technology_2019_EN_download_version2.pdf].

[2] Ballif, C. et al. 2019, "Solving all bottlenecks for silicon heterojunction technology", *Photovoltaics International*, 42nd Edition, p. 85.

[3] Frank, G. & Köstlin, H. 1982, "Electrical properties and defect model of tin-doped indium oxide layers", *Appl. Phys. A,* Vol. 27, No. 4, pp. 197–206 [https://doi.org/10.1007/BF00619080].

[4] Hamberg, I. & Granqvist, C.G. 1986, "Evaporated Sn doped In_2O_3 films: Basic optical properties and applications to energy efficient windows", *J. Appl. Phys.,* Vol. 60, No. 11, pp. R123–R160 [https://doi.org/10.1063/1.337534].

[5] Balestrieri, M. et al. 2011, "Characterization and optimization of indium tin oxide films for heterojunction solar cells", *Sol. Energy Mater. Sol. Cells,* Vol. 95, No. 8, pp. 2390–2399 [https://doi.

"Scaling and increasing the throughput of TCO production lines is the way to go."

org/10.1016/j.solmat.2011.04.012].
[6] Koida, T. & Kondo, M. 2007, "Comparative studies of transparent conductive Ti-, Zr-, and Sn-doped In_2O_3 using a combinatorial approach", *J. Appl. Phys.,* Vol. 101, No. 6, p. 063713 [https://doi.org/10.1063/1.2712161].
[7] Kobayashi, E., Watabe, Y. & Yamamoto, T. 2015, "High-mobility transparent conductive thin films of cerium-doped hydrogenated indium oxide", *Appl. Phys. Expr.,* Vol. 8, No. 1, p. 015505 [https://doi.org/10.7567/APEX.8.015505].
[8] Macco, B. et al. 2014, "High mobility In_2O_3:H transparent conductive oxides prepared by atomic layer deposition and solid phase crystallization", *physica status solidi (RRL),* Vol. 8, No. 12, pp. 987–990 [https://doi.org/10.1002/pssr.201409426].
[9] Erfurt, D. et al. 2019, "Improved electrical properties of pulsed DC magnetron sputtered hydrogen doped indium oxide after annealing in air", *Mater. Sci. Semicon. Proc.,* Vol. 89, pp. 170–175 [https://doi.org/10.1016/j.mssp.2018.09.012].
[10] Yu, J. et al. 2016, "Tungsten doped indium oxide film: Ready for bifacial copper metallization of silicon heterojunction solar cell", *Sol. Energy Mater. Sol. Cells,* Vol. 144, pp. 359–363 [https://doi.org/10.1016/j.solmat.2015.09.033].
[11] Newhouse, P.F. et al. 2005, "High electron mobility W-doped In_2O_3 thin films by pulsed laser deposition", *Appl. Phys. Lett.,* Vol. 87, No. 11, p. 112108 [https://doi.org/10.1063/1.2048829].
[12] Asikainen, T., Ritala, M. & Leskelä, M. 2003, "Atomic layer deposition growth of zirconium doped In_2O_3 films", *Thin Solid Films*, Vol. 440, No. 1, pp. 152–154 [https://doi.org/10.1016/S0040-6090(03)00822-8].
[13] Morales-Masis, M. et al. 2018, "Highly conductive and broadband transparent Zr-doped In_2O_3 as front electrode for solar cells", *IEEE J. Photovolt.,* pp. 1–6 [https://doi.org/10.1109/JPHOTOV.2018.2851306].
[14] Morales-Masis, M. et al. 2017, "Transparent electrodes for efficient optoelectronics", *Adv. Electron. Mater.,* Vol. 3, No. 5, p. 1600529 [https://doi.org/10.1002/aelm.201600529].
[15] Delahoy, A.E. & Guo, S.Y. 2005, "Transparent and semitransparent conducting film deposition by reactive-environment, hollow cathode sputtering", *J. Vac. Sci. Technol. A,* Vol. 23, No. 4, pp. 1215–1220 [https://doi.org/10.1116/1.1894423].
[16] van Hest, M.F.A.M. et al. 2005, "Titanium-doped indium oxide: A high-mobility transparent conductor", *Appl. Phys. Lett.,* Vol. 87, No. 3, p. 032111 [https://doi.org/10.1063/1.1995957].
[17] Meng, Y. et al. 2001, "A new transparent conductive thin film In_2O_3:Mo", *Thin Solid Films*, Vol. 394, No. 1–2, pp. 218–222 [https://doi.org/10.1016/S0040-6090(01)01142-7].
[18] Yoshida, Y. et al., "Development of radio-frequency magnetron sputtered indium molybdenum oxide", *J. Vac. Sci. Technol. A,* Vol. 21, No. 4, pp. 1092–1097 [https://doi.org/10.1116/1.1586281].
[19] Warmsingh, C. et al. 2004, "High-mobility transparent conducting Mo-doped In_2O_3 thin films by pulsed laser deposition", *J. Appl. Phys.,* Vol. 95, No. 7, pp. 3831–3833 [https://doi.org/10.1063/1.1646468].
[20] Ruske, F. et al. 2010, "Improved electrical transport in Al-doped zinc oxide by thermal treatment", *J. Appl. Phys.,* Vol. 107, No. 1, p. 013708 [https://doi.org/10.1063/1.3269721].
[21] Hüpkes, J. et al. 2014, "Damp heat stable doped zinc oxide films", *Thin Solid Films,* Vol. 555, pp. 48–52 [https://doi.org/10.1016/j.tsf.2013.08.011].
[22] Greiner, D. et al. 2011, "Damp heat stability of Al-doped zinc oxide films on smooth and rough substrates", *Thin Solid Films*, Vol. 520, No. 4, pp. 1285–1290 [https://doi.org/10.1016/j.tsf.2011.04.190].
[23] Morales-Vilches, A.B. et al. 2018, "ITO-free silicon heterojunction solar cells with ZnO:Al/SiO_2 front electrodes reaching a conversion efficiency of 23%", *IEEE J. Photovolt.,* Vol. 9, No. 1, pp. 1–6 [https://doi.org/10.1109/JPHOTOV.2018.2873307].
[24] Bivour, M. et al. 2014, "Silicon heterojunction rear emitter solar cells: Less restrictions on the optoelectrical properties of front side TCOs", *Sol. Energy Mater. Sol. Cells,* Vol. 122, pp. 120–129 [https://doi.org/10.1016/j.solmat.2013.11.029].
[25] Basset, L. et al. 2018, "Series resistance breakdown of silicon heterojunction solar cells produced on CEA-INES pilot line", *Proc. 35th EU PVSEC*, Brussels, Belgium, pp. 721–724 [https://doi.org/10.4229/35thEUPVSEC20182018-2DV.3.21].
[26] Ling, Z.P. et al. 2015, "Three-dimensional numerical analysis of hybrid heterojunction silicon wafer solar cells with heterojunction rear point contacts", *AIP Adv.,* Vol. 5, No. 7, p. 077124 [https://doi.org/10.1063/1.4926809].
[27] Cruz, A. et al. 2019, "Effect of front TCO on the performance of rear-junction silicon heterojunction solar cells: Insights from simulations and experiments", *Sol. Energy Mater. Sol. Cells,* Vol. 195, pp. 339–345 [https://doi.org/10.1016/j.solmat.2019.01.047].
[28] Wang, E.-C. et al. 2019, "A simple method with analytical model to extract heterojunction solar cell series resistance components and to extract the A-Si:H(i/p) to transparent conductive oxide contact resistivity", *AIP Conf. Proc.,* Vol. 2147, No. 1, p. 040022 [https://doi.org/10.1063/1.5123849].
[29] Cruz, A. et al. 2019, "Influence of silicon layers on the growth of ITO and AZO in silicon heterojunction solar cells", *IEEE J. Photovolt.,* pp. 1–7 [https://doi.org/10.1109/JPHOTOV.2019.2957665].
[30] Muñoz, D. & Roux, D. 2019, "The race for high efficiency in production: Why heterojunction is now ready for market", *Proc. 36th EU PVSEC*, Marseille, France, pp. 1–20.
[31] Strahm, B. et al. 2019, "'HJT 2.0' performance improvements and cost benefits for silicon heterojunction cell production", *Proc. 36th EU PVSEC,* Marseille, France, pp. 300–303 [https://doi.org/10.4229/EUPVSEC20192019-2EO.1.3].
[32] Zhang, D. et al. 2013, "Design and fabrication

of a SiO_x/ITO double-layer anti-reflective coating for heterojunction silicon solar cells", *Sol. Energy Mater. Sol. Cells,* Vol. 117, pp. 132–138 [https://doi.org/10.1016/j.solmat.2013.05.044].
[33] Geissbühler, J. et al. 2014, "Silicon heterojunction solar cells with copper-plated grid electrodes: Status and comparison with silver thick-film techniques", *IEEE J. Photovolt.,* Vol. 4, No. 4, pp. 1055–1062 [https://doi.org/10.1109/JPHOTOV.2014.2321663].
[34] Herasimenka, S.Y. et al. 2016, "ITO/SiO_x:H stacks for silicon heterojunction solar cells", *Sol. Energy Mater. Sol. Cells,* Vol. 158, Part 1, pp. 98–101 [https://doi.org/10.1016/j.solmat.2016.05.024].
[35] Santbergen, R. 2016, "Manual for solar cell optical simulation software: GENPRO4", Photovoltaic Materials and Devices, Delft University of Technology.
[36] Haschke, J. et al. 2020, "Lateral transport in silicon solar cells", *J. Appl. Phys.,* Vol. 127 [https://doi.org/10.1063/1.5139416].
[37] Bivour, M. et al. 2012, "Improving the a-Si:H(p) rear emitter contact of n-type silicon solar cells", *Sol. Energy Mater. Sol. Cells,* Vol. 106, pp. 11–16 [https://doi.org/10.1016/j.solmat.2012.06.036].
[38] Procel, P. et al. 2018, "Theoretical evaluation of contact stack for high efficiency IBC-SHJ solar cells", *Sol. Energy Mater. Sol. Cells,* Vol. 186, pp. 66–77 [https://doi.org/10.1016/j.solmat.2018.06.021].
[39] Luderer, C. et al. 2019, "Contact resistivity of the TCO/a-Si:H/c-Si heterojunction", *Proc. 36th EU PVSEC,* Marseille, France, pp. 538–540 [https://doi.org/10.4229/EUPVSEC20192019-2DV.1.48].
[40] Messmer, C. et al. 2019, "Influence of interfacial oxides at TCO/doped Si thin film contacts on the charge carrier transport of passivating contacts", *IEEE J. Photovolt.,* pp. 1–8 [https://doi.org/10.1109/JPHOTOV.2019.2957672].
[41] Cox, R.H. & Strack, H. 1967, "Ohmic contacts for GaAs devices", *Solid-State Electron.,* Vol. 10, No. 12, pp. 1213–1218 [https://doi.org/10.1016/0038-1101(67)90063-9].
[42] Fellmeth, T., Clement, F. & Biro, D. 2014, "Analytical modeling of industrial-related silicon solar cells", *IEEE J. Photovolt.,* Vol. 4, No. 1, pp. 504–513 [https://doi.org/10.1109/JPHOTOV.2013.2281105].

About the Authors

Alexandros Cruz received his master's in renewable energy systems from the Berlin Institute of Technology in 2013. From 2013 to 2016 he worked at SolarWorld in the Module Technology department, focusing on module processing R&D. He subsequently joined the Helmholtz-Zentrum Berlin to pursue his Ph.D., with a thesis topic on TCO implementation in SHJ solar cells.

Dr. Darja Erfurt received her Ph.D. from the Technical University of Berlin in 2019 for her work on high-mobility TCOs in chalcopyrite thin-film solar cells. She is currently a postdoctoral researcher at HZB, where she focuses on SHJ solar cells.

René Köhler has 10 years' experience in the crystalline silicon PV industry, and began his career at SolarWorld Innovations, working on PERC and TOPCon/POLO. He then worked in the area of SHJ solar cells at the Helmholtz-Zentrum Berlin, before joining VON ARDENNE in 2018. He holds a Diploma degree in technical physics from the Technical University of Ilmenau.

Dr.-Ing. Martin Dimer received his Ph.D. from the Technical University of Braunschweig. Since 1996 he has been working at VON ARDENNE in various positions, including project manager, group leader and expert in the field of thin-film coatings based on PVD and PECVD technologies. Today, his main focus of activity is thin-film technology for PV.

Dr. Eric Schneiderlöchner began his career in PV in 2000 at Fraunhofer ISE, where he also worked on his Ph.D. He then gained 12 years' experience in various engineering and management roles in solar cell manufacturing and process engineering at the former Germany-based solar company SolarWorld. He is currently the director of Crystalline Photovoltaics Technology at the German vacuum equipment provider VON ARDENNE GmbH.

Prof. Dr. Bernd Stannowski received his Ph.D. in 2002 from Utrecht University in the Netherlands. From 2003 to 2010 he worked in the PV industry and was involved in R&D on thin-film silicon solar cells, as well as in PV module production. Since 2010 he has been with the PVcomB at Helmholtz-Zentrum Berlin, where he leads the Silicon Solar Cells group.

Enquiries

Bernd Stannowski
Helmholtz-Zentrum Berlin, PVcomB
Schwarzschildstr. 3
12489 Berlin, Germany

Tel: +49-30-8062-15491
Email: bernd.stannowski@helmholtz-berlin.de
Website: www.helmholtz-berlin.de, www.pvcomb.de